Direct Numerical Simulation of Non-Linear Transitional Stages in an Experimentally Investigated Laminar Separation Bubble

Olaf Marxen and Ulrich Rist

Institut für Aerodynamik und Gasdynamik, Universität Stuttgart
olaf.marxen@iag.uni-stuttgart.de

Summary: This paper details a joint numerical and experimental effort to investigate a transition process in a laminar separation bubble, with the emphasis being put on the numerical contribution. A laminar separation bubble is formed if a laminar boundary layer separates in a region of adverse pressure gradient on a flat plate and undergoes transition, leading to a reattached turbulent boundary layer. Development of disturbances during the transition process in such a separation bubble is studied by means of direct numerical simulation with controlled disturbance input. Focus is put on the stage of non-linear development of these perturbations, for which a detailed comparison between numerical and experimental results is given. Beside physical phenomena like shear-layer roll-up and vortex shedding, computational aspects such as the performance of the numerical code on supercomputers are treated.

1 Introduction

Transition to turbulence in a two-dimensional separated boundary layer often leads to reattachment of the turbulent boundary layer and the formation of a laminar separation bubble (LSB). In environments with a low level of disturbances fluctuating in time, the transition process is governed by strong amplification of these disturbances. Such a scenario is typical for a pressure-induced LSB, e.g. found on a (glider) wing in free flight, or for an experiment where the region of pressure rise is preceded by a favorable pressure gradient that damps out unsteady perturbations (Watmuff, 1999). In the region of an adverse pressure gradient, disturbance waves are subject to strong amplification, and their saturation marks the location of transition to turbulence.

Laminar-turbulent transition in laminar separation bubbles has been the subject of numerous studies in the past. Only some of the most recent ones will be mentioned here. Watmuff (1999) carried out an experimental study of

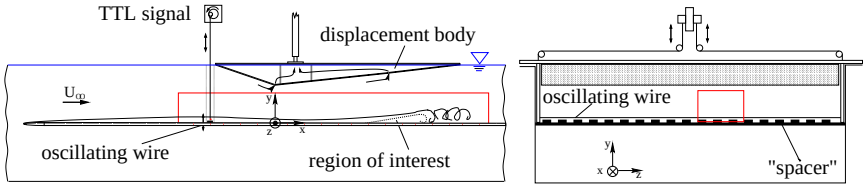

Fig. 1. Configuration for the experiment by Lang (2005) – sketch (provided by Matthias Lang) of the test section of the laminar water tunnel at the IAG

a LSB, while Spalart & Strelets (2000), Alam & Sandham (2000), Maucher *et al.* (2000), and Wissink & Rodi (2004) tackled the flow by means of direct numerical simulations (DNS). Most of the cited studies conclude that some type of linear instability (Tollmien-Schlichting or Kelvin-Helmholtz instability) is the cause for transition.

With the rise of computational fluid dynamics during the last decades, and especially with the availability of large (vector-)supercomputers, there also came up a cry to verify numerical simulations not only within themselves, e.g. by means of grid-refinement studies, but also by a comparison with the outcomes of available experiments. For flows with physical processes as complex as in a laminar separation bubble, a comparison of *only* time-averaged and root-mean-square quantities appears of little value and cannot be considered a true verification. Rather, a detailed quantitative time-accurate comparison of numerical results and experimental data obtained in a LSB is required. Both, experimental and numerical methods have certain, but different, weaknesses that make a meaningful comparison quite demanding.

This paper shall serve to demonstrate that the numerical method used within the project LAMTUR is capable to provide realistic space- and time-accurate simulations even of non-linear stages of the transition process in a laminar separation bubble. The method was adapted to represent a physical situation as given in Fig. 1, for which an experimental realization is available. The experiment was planned in a way as to minimize numerical difficulties as far as possible. A crucial point thereby is the explicit forcing of disturbances, so that the flow is not governed by the (hard to determine) background disturbances in the very tunnel that was used for the experiment.

The whole project LAMTUR aims at evaluating transition mechanisms in wall-bounded flows – in the present 'subproject' in a LSB – and is motivated by several considerations. Identifying the relevant disturbances and understanding their role in the transition process is a necessary condition for the prediction of transition in similar flows. In addition, it can be viewed as a first step towards control of the underlying flow field.

Here, the outcomes of a large-scale computation will be described. Physical insights gained within the subproject are discussed in more detail in Marxen *et al.* (2003, 2004, 2005); Marxen (2005). All calculations rely on a single case and mainly serve to illustrate transitional processes that *can* occur in a LSB.

2 Description of the Flow Field

The present case is defined by an experimental set-up specified in detail in Lang *et al.* (2004), Lang (2005). A sketch of the set-up was given in Fig. 1. Only a brief description is given here. The set-up was used during several measurement campaigns carried out by Matthias Lang at the Institut für Aerodynamik und Gasdynamik, Universität Stuttgart. Outcomes of these campaigns are taken for comparison with computational results throughout this paper. Specifically, results from measurements by means of Laser-Doppler Anemometry in 2000, denoted as *LDA (2000)* in the following, and 2001, *LDA (2001)*, as well as those obtained from Particle Image Velocimetry in 2001, *PIV (2001)*, are used.

2.1 General Parameters

A flat plate is mounted in the free stream ($\breve{U}_\infty$=$0.125\,m/s$) of the test section of a laminar water tunnel ($\breve{\nu}$=$10^{-6}\,m^2/s$). A streamwise pressure gradient is imposed locally on the flat-plate boundary layer by a displacement body (length of the body $\breve{L}_{DB}^{Exp}$=$0.69\,m$), inducing a region of favorable pressure gradient followed by a pressure rise. The origin of the coordinate system corresponds to the narrowest cross section beneath the displacement body.

In the region of adverse pressure gradient (starting at $\breve{x} \approx 0\,m$), a laminar separation bubble develops. The transition experiment is performed with controlled disturbance input. A 2-d time-harmonic perturbation is introduced upstream of the displacement body (at $\breve{x}$=$-0.23\,m$) by an oscillating wire (fundamental frequency $\breve{f}_0$=$1.1\,s^{-1}$). Additionally, 3-d disturbances are imposed by placing thin (height: $10^{-3}\,m$) metal plates, so-called spacers, regularly underneath the wire (fundamental spanwise wavelength $\breve{\lambda}_z$=$0.058\,m$).

All quantities are non-dimensionalized. The global reference length is chosen to be $\breve{L}_{ref}$=$^2/_3\,m \approx \breve{L}_{DB}^{Exp}$. The reference velocity is evaluated at a streamwise position where the flow field is still not strongly affected by the downstream presence of the separation bubble, yet already influenced by the displacement body. It was found that x=-0.15 is a convenient location for that purpose, since at that position only small wall-normal changes of the streamwise velocity are observable outside the boundary layer. Thus, the reference velocity amounts to $\breve{U}_{ref}$=$0.15\,m/s \approx 1.2 \cdot \breve{U}_\infty$, resulting in a global Reynolds number $Re_{global} = 10^5$ in water. For DNS calculations, general physical parameters of the flow (see Table 1) are chosen to match the experimental set-up as closely as possible.

At the streamwise position of the inflow boundary x_{ifl}=-0.6, the measured boundary-layer profile can be approximated by a Falkner-Skan similarity solution with $Re_{\delta_1,ifl}$=900 and $\beta_{H,ifl}$=0.13. The outflow boundary is located at x_{ofl}=1.16 with a preceeding damping region starting at $x_{st,oBZ}$=0.9911. The useful region of the integration domain extends up to x≈0.95.

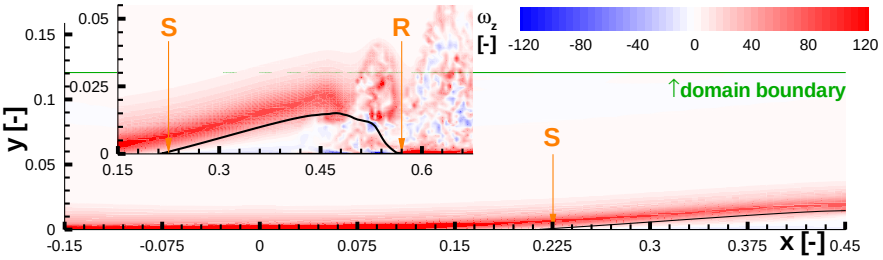

Fig. 2. Contours of the time- and spanwise-averaged spanwise vorticity $\bar{\omega}_z$ from DNS together with mean dividing streamline $\bar{\psi} = 0$. In the insert, the wall-normal direction is enlarged by a factor of 4 and an instantaneous view of ω_z is given

The pressure gradient is prescribed via streamwise and wall-normal velocity distributions $u_e(x), v_e(x)$ at a height y_{max}=0.1207. These distributions are chosen guided by potential(slip)-flow distributions u_{slip}, v_{slip}, but slightly adapted to compensate for errors introduced through the assumptions in deriving the potential-flow solution and to obtain the best possible overall matching of the DNS results with the experiment. The slip flow was estimated from experimental mean values $\bar{u}_{exp}$, $\bar{v}_{exp}$ at constant y=0.06. The procedure used to derive slip velocities from measured data is given in Marxen (2005). A rough estimate of the pressure-gradient parameter gives P=$\breve{\delta}_2/\breve{\nu} \cdot \partial\breve{u}_{slip}/\partial\breve{x}|_{Separation} \approx -0.32$.

It was not possible to obtain a steady-state solution to the Navier-Stokes equations with the chosen distribution $u_e(x)$, $v_e(x)$, i.e. the actual flow field observable downstream of transition is highly unsteady from x=0.48 onwards. For that reason, the subsequent discussion of the mean flow field is restricted to the laminar part of the LSB ($x \leq 0.45$).

2.2 Mean Flow and Boundary-Layer Properties

Contours of the spanwise vorticity ω_z are shown in Fig. 2, together with the mean dividing streamline $\bar{\psi}$=0. A fairly large but shallow separation region has developed. Its start is marked by the point of separation S ($x_S \approx 0.225$). To provide an impression of the size of the LSB, the whole bubble is included in the insert of Fig. 2, and the mean reattachment point is marked by R.

Table 1. Simulation parameters for DNS

$\breve{U}_{ref}$	$0.15\,m/s$	$\breve{\nu}$	$10^{-6}\,m^2/s$	Re_{global}	10^5	$Re_{\delta_{1,ifl}}$	900
y_{max}	0.1207	β_0	30.7	γ_0	72	$\beta_{H,ifl}$	0.13
x_{ifl}	-0.6	x_{ofl}	1.16	$x_{st,oBZ}$	0.9911	$x_{en,oBZ}$	1.1586
NMAX	2690	MMAX	241	KMAX	63	LPER	1200

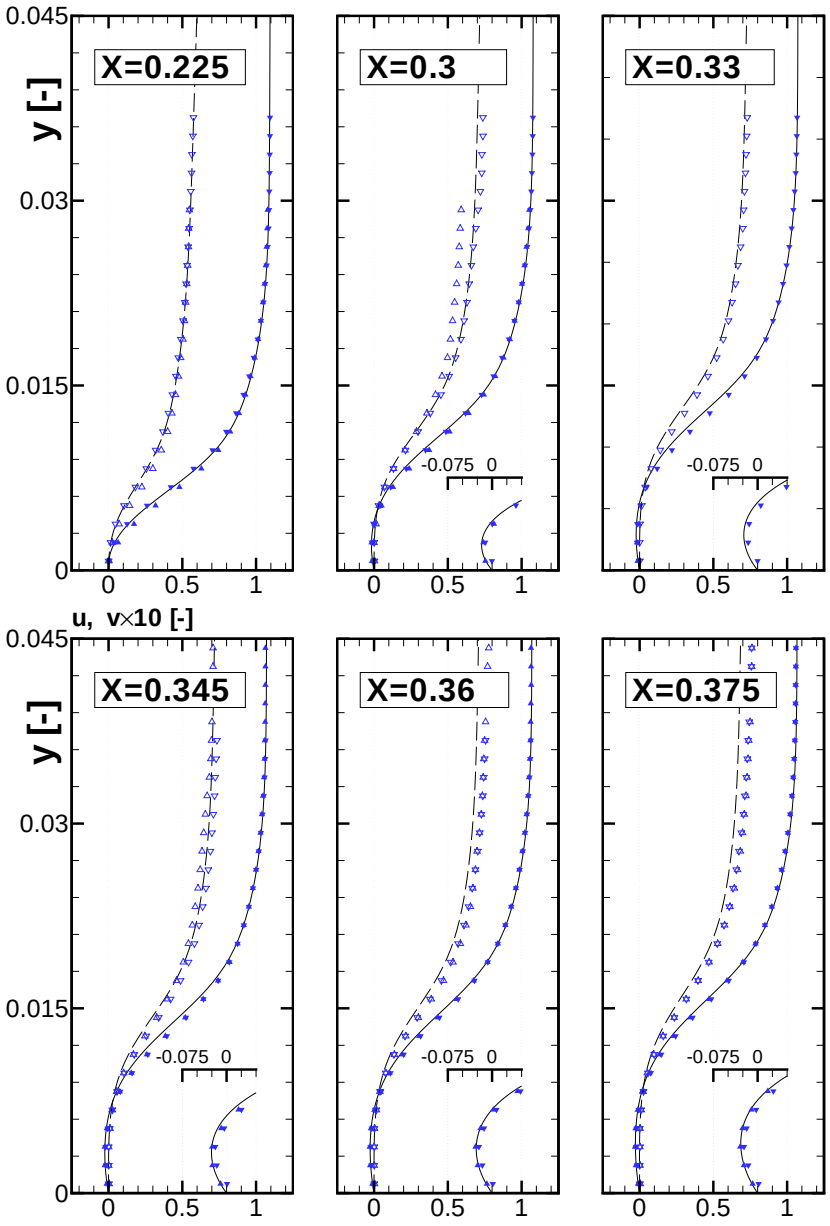

Fig. 3. Time- and spanwise-averaged streamwise (solid lines/filled symbols) and wall-normal (dashed lines/open symbols) velocity profiles at several streamwise positions in the laminar part of the LSB. Comparison of DNS (lines), LDA (2001) (deltas), and LDA (2000) (gradients). Inserts show u in the reverse-flow region enlarged by a factor of 4

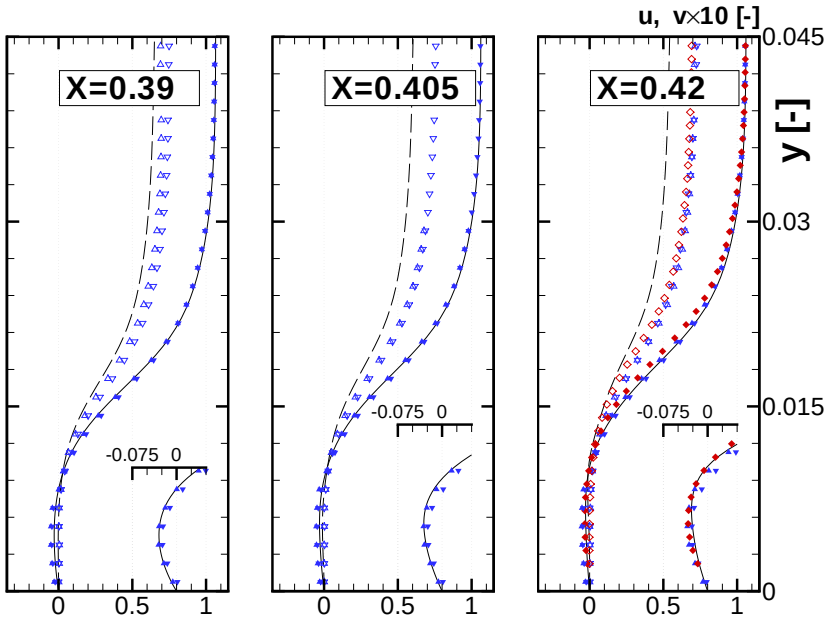

Fig. 4. Same as Fig. 3, except that streamwise positions x=0.39, 0.405, and 0.42 are shown. Comparison of DNS (lines), LDA (2001) (deltas), LDA (2000) (gradients), and PIV (2001) (diamonds)

Figs. 3 and 4 compare time- and spanwise-averaged velocity profiles at separation and in the reverse-flow region. Satisfactory agreement between DNS results and measurements for all streamwise positions even for the small wall-normal velocity component (note the different scaling for u and v in the figures) reveals that a separation bubble of approximately the same height is formed. The inserts showing the reverse-flow region of the LSB confirm that a comparable amount of reverse flow exists in the DNS and in the experiment. The last x-position shown is close to the transition location.

Boundary-layer quantities from DNS are computed using a pseudo velocity that is obtained by integrating the spanwise vorticity in wall-normal direction (see Spalart & Strelets, 2000). Figs. 5 and 6 show the streamwise development of important boundary-layer parameters. A strong increase in the quantities related to the displacement of the boundary layer (such as the displacement thickness δ_1 or Re_{δ_1}) is visible in the separated region.

In Fig. 5, the pressure coefficient at the wall in case of slip flow $c_{p,slip}$ serves to illustrate the development of a pressure plateau due to the LSB. Comparing c_p obtained from potential-flow theory and from DNS, one can see that deviation of the pressure distribution is not restricted to the region around separation, but already visible far upstream from it. This can be attributed to the presence of the separation bubble (Marxen, 2005).

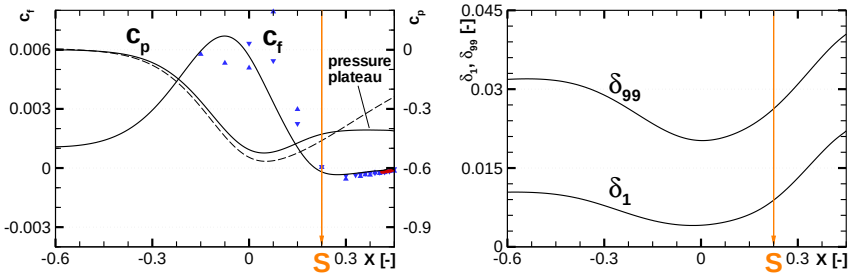

Fig. 5. Coefficients for surface pressure c_p, skin friction c_f (left), and boundary-layer thicknesses δ_1, δ_{99} (right). Comparison of DNS (solid lines), slip-flow (potential-flow theory) results $c_{p,slip}$ (dashed line), LDA (2001) (deltas), LDA (2000) (gradients), and PIV (2001) (diamonds)

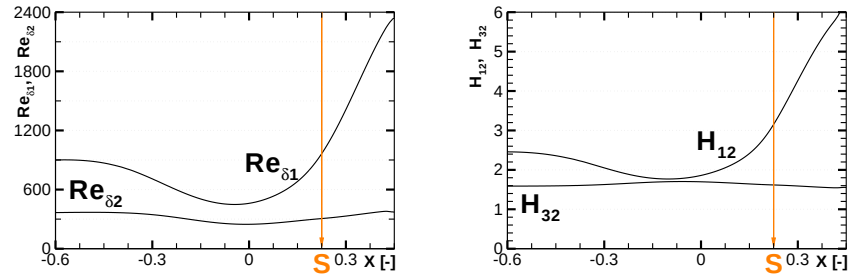

Fig. 6. Reynolds numbers Re_{δ_1} and Re_{δ_2} (left). Shape factors H_{12} and H_{32} (right)

2.3 Post-Processing of Time-Dependent Results

A double Fourier transform in time and spanwise direction of data sets from measurements or simulations yields disturbance amplitudes and phases. Below, the notation (h, k) will be used to specify the modes, with h and k denoting wave-number coefficients in time and spanwise direction, respectively.

In the simulations, the separation bubble showed low-frequency oscillations (so-called flapping) so that the Fourier analysis had to be carried out using a Hanning-window function to suppress aliasing effects. The amplitude of the subharmonic *after* using a Hanning-window was considerably lower than before and this was taken as proof that frequencies of the flapping and of the vortex shedding (see below) were indeed well separated. Four periods of the fundamental frequency where used in the analysis. The flow field is advanced in time until a quasi-periodic state is reached.

2.4 Linear Disturbance Evolution

Linear disturbance evolution in the considered flow shall only briefly be summarized – a detailed treatment can be found in Marxen *et al.* (2004, 2005);

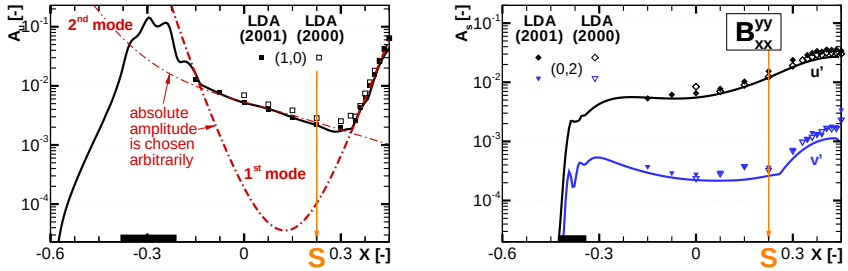

Fig. 7. Amplification curves for the maximum (in y) velocity fluctuations $|\hat{u}'^{(\mathrm{h,k})}_{max}|$, $|\hat{v}'^{(\mathrm{h,k})}_{max}|$. Left: 2-d mode $(1,0)$ from DNS (solid line); LST (dash-dotted lines): first (thick), second (thin) mode; measurements LDA (2001) (filled symbols), LDA (2000) (open symbols). Right: steady 3-d mode $(0,2)$ from DNS (lines) together with measurements LDA (2001) (filled symbols), LDA (2000) (open symbols)

Marxen (2005). All the results presented in this subsection have been obtained by means of a disturbance-flow computation (see Sect. 4), making use of the flow described in the last subsection as a base flow.

Linear stability theory (LST) based on the Orr-Sommerfeld equation (Schlichting, 1979) predicts that a discrete spectrum of eigensolutions exists for a certain velocity profile. For transition in low disturbance-level environments, out of these only the least damped, or most amplified, disturbance eigenmodes are relevant. An analysis of the stability characteristics for this flow field (Marxen, 2005) revealed that solely a single 2-d mode, here denoted as *first mode*, becomes amplified in the region of adverse pressure gradient, while at the same time precisely this mode is stronger damped in the acceleration region than another one, the *second mode*, existing in the flow.

In a numerical simulation or in the experiment, *all* eigenmodes with the respective frequency will inevitably be excited, though with different initial amplitude. For the present position of the oscillating wire in the experiment (x=−0.345), the second mode is initially visible, while further downstream the first one becomes dominant (Fig. 7, left). Therefore, it is sufficient to excite this first mode only in the DNS, e.g. with a disturbance strip placed in the location of pressure minimum (x=0) as it will be described below.

The evolution of a different class of linear disturbances – steady, three-dimensional ones – is shown in Fig. 7, right. A detailed discussion of this type of disturbance can be found in Marxen *et al.* (2004); Marxen (2005); Marxen *et al.* (2005). The initial behavior of mode $(0,2)$ in the region of favorable pressure gradient is associated with optimal transient growth, while further downstream a generic growth that is independent on initial condition can be observed. Again, good agreement of numerical and experimental results is visible. The two perturbations just discussed, the 2-d Tollmien-Schlichting wave and the 3-d steady streak, are the dominating disturbances up to the onset of non-linear stages of the transition process.

3 Non-linear Disturbance Evolution

Emphasis will be put now on the early non-linear stages for unsteady perturbations, i.e. stages where saturation and mutual interaction of disturbances occur for the first time. This restriction justifies to consider only spanwise symmetric perturbations.

Saturation of the disturbance waves leads to shear-layer roll-up and vortex shedding as it will be illustrated in the following. This vortex shedding is often essentially a two-dimensional phenomenon (i.e. strong spanwise coherence of the vortex structure), caused by either spanwise constant (2-d) small-amplitude waves, as it is the case here, or by spanwise-harmonic (3-d) waves with small obliqueness angles in an otherwise undisturbed flow.

Disturbances are forced via blowing and suction at the wall through a disturbance strip. The position and amplitude of the disturbance input for the simulation is given in Table 2. The fundamental frequency is β_0=30.7 and the fundamental spanwise wavenumber γ_0=72.0. Note that the disturbance strip is placed further downstream, i.e. not at the location of the oscillating wire in the experiment, due to the reasoning given in the last section.

Growth of a strongly oblique wave (mode $(1,2)$) – despite its approximately neutral linear stability (Marxen *et al.*, 2004; Marxen, 2005) – is treated in Sect. 3.1. With the saturation of the fundamental, primarily amplified disturbances, non-linearly generated higher harmonics fill-up the disturbance spectrum in time (higher h) and span (higher k). This effect is discussed in Sect. 3.2 exemplarily for the two-dimensional perturbations.

3.1 Growth of Oblique Disturbances

Strong growth of mode $(1,2)$ inside the LSB is a result of non-linear generation, i.e. interaction of modes $(1,0) \times (0,2)$ and not due to a secondary instability, as proven by a variation in excitation amplitude of modes $(0,2)$ and $(1,2)$ in Marxen *et al.* (2004). Such a non-linear generation is seen to provide the experimentally observed growth rate (Fig. 8, left). Final growth and saturation of mode $(1,2)$ has to be attributed to an independent evolution of this mode. Equal behavior of the most relevant modes for the linear (thin lines) and non-linear (thick lines) computations verifies the applicability of the disturbance formulation discussed in Sect. 2.4.

Table 2. Forcing amplitudes A_v and location of the disturbance strip

	$(1,0)$	$(1,1)$
A_v	$1.15 \cdot 10^{-5}$	0.026
disturbance strip: $x \in$	$[-0.0352, 0.0486]$	$[-0.4702, -0.3833]$

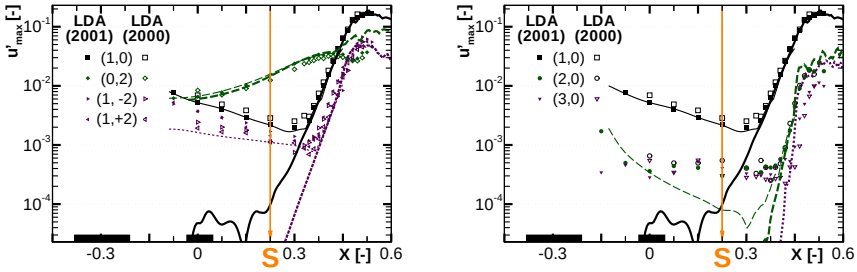

Fig. 8. Amplification curves for the maximum (in y) streamwise velocity fluctuation $|\hat{u}'^{(h,k)}_{max}|$. DNS results for linear (thin lines) and non-linear (thick lines) simulations; measurements LDA (2001) (filled symbols), LDA (2000) (open symbols)

3.2 Non-linear Generation, Shear-layer Roll-up, and Vortex-shedding

A comparison of the evolution of mode $(1,0)$ in the linear and non-linear simulations (Fig. 8) reveals that instead of exciting both least-damped linear eigenmodes as discussed before, one can as well make sure that only the amplified first mode is visible by relocating the disturbance strip in the region around the pressure minimum (x=0). This does not alter the evolution of perturbation $(1,0)$ deeper inside the LSB for x>0.36.

Comparing the DNS data with measurements (Fig. 8, right) it can be seen that in case of the experiment, mode $(2,0)$ is not non-linearly generated by the fundamental disturbance in the interval $x \in [0, 0.375]$, but either possesses its own evolution or can be attributed to the accuracy-limit of the LDA. Outside this interval, and in particular deeper inside the LSB, mode $(2,0)$ is indeed a true higher harmonic of the fundamental perturbation. The DNS is able to predict roughly the same location and amplitude level of disturbance saturation as observed experimentally for the unsteady disturbances (Fig. 8).

To illustrate the physical meaning of the saturation of the most relevant modes and the corresponding gain in amplitude of higher harmonics, we switch to the viewpoint in physical space, since the stage following disturbance saturation is associated with the development of coherent structures. In this stage, the phases and amplitudes of perturbations relative to each other are important, therefore it is convenient to look at them in physical space.

Reduction of information to a manageable level comes from looking at a single spanwise position only. Fig. 9 reveals that the non-linear processes given in Fourier space in Fig. 8 are associated with a roll-up of the separated shear-layer, i.e. the modes synchronize in a way as to form a spanwise vortex. The resulting vortex pumps outer, high-speed fluid towards the wall until it detaches from the shear layer and is shed downstream with fundamental frequency. This process is responsible for the reattachment of the flow in the mean.

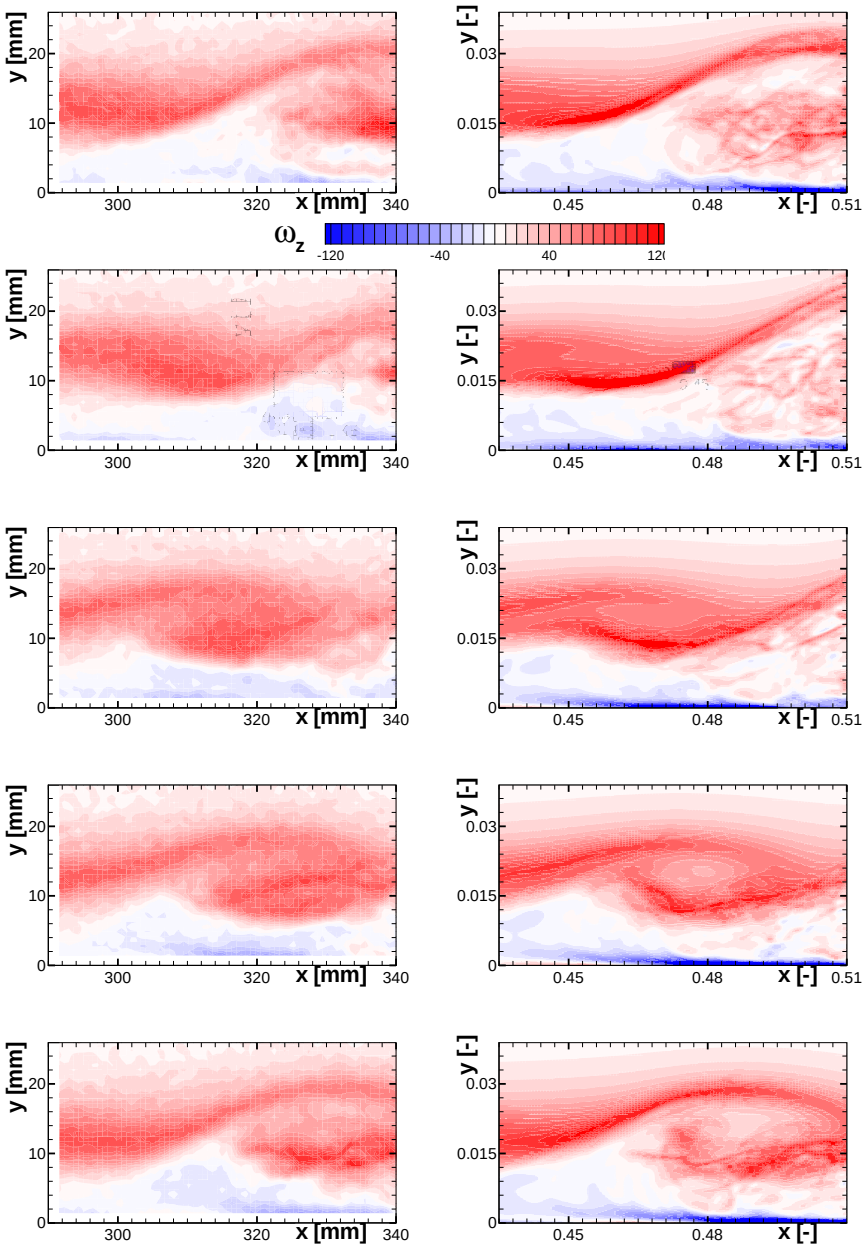

Fig. 9. Contours (levels: ω_z=−120 . . . 120, Δ=8) of the spanwise vorticity at z=0 for single time instants (from top to bottom: t/T_0=0, 0.2, 0.4, 0.6, 0.8). Comparison of phase-averaged ($T_{aver} \geq 20$) results from PIV (2001) (left) and DNS (right)

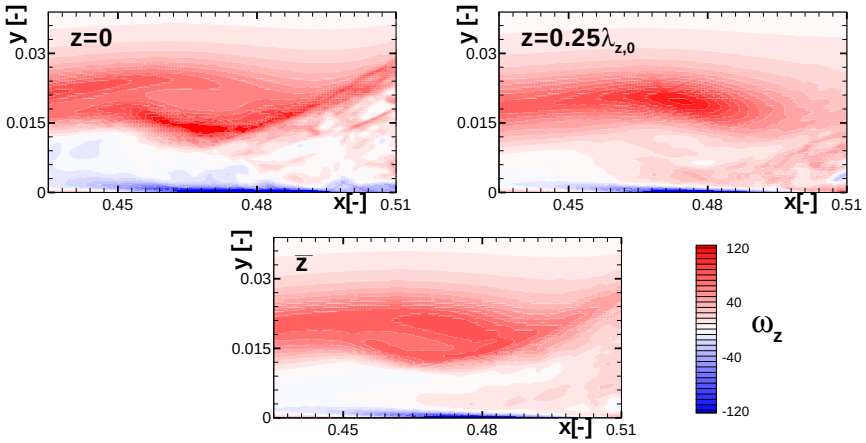

Fig. 10. Contours (levels: ω_z=−120 . . . 120, Δ=8) of the phase-averaged (T_{aver}=20) spanwise vorticity at t/T_0=0.4 from DNS. Comparison of peak z=0 (upper left), valley z=0.25$\lambda_{z,0}$ (upper right) position, and spanwise average (center)

However, the shear-layer roll-up is modulated in spanwise direction (Fig. 10). Even though we do not have an exact modulation of boundary-layer thickness caused by mode $(0, 2)$, still for $x < 0.45$ at some spanwise positions the top of the shear layer is closer to the wall (z=0.25$\lambda_{z,0}$), while at others it is further away (z=0). For that reason, Lang *et al.* (2001) denote this as a peak and valley structure similar to e.g. K-type breakdown. The fact that mode $(1, 0)$ is seen to possess the largest amplitude around and even after saturation (Fig. 8) – compared to 3-d modes – suggests that the 2-d structure mainly corresponding to this mode, i.e. the formation of the spanwise vortex, is dominant in the flow. This is confirmed by looking at Fig. 10, where it can be seen that the spanwise local evolution at peak and valley positions resembles each other as well as the spanwise average.

4 Computational Aspects

Simulation cases are set-up in a way as to economically apply available computational resources, relying on supercomputers only when it is essential. To maximize the physical outcomes with a minimum in computational effort, the following strategy was pursued: one large-scale computation was followed by several smaller ones and by theoretical investigations. The large-scale computation was carried out in total-flow formulation (the standard formulation typically used in CFD) to reproduce the experiment as closely as possible, and results of that computation have been presented in detail in Sect. 3 (denoted before as non-linear simulation). Based on the resulting flow field (after time averaging, i.e. the one described in Sect. 2.2), several smaller computations

Table 3. Performance of *n3d* in the present case for a typical run

Machine	CPU×Nodes	GFLOPS/CPU	Memory	CPU Time/Period
NEC SX-6	8×1	3.06	5.68 GB	$30.79\,h$
NEC SX-8	8×1	5.38	6.19 GB	$16.78\,h$
NEC SX-8, MPI	8×2	4.29	8.96 GB	$21.17\,h$

could be run in disturbance formulation (before denoted as linear computations, see Sect. 2.4) with varying disturbance input. In addition, theoretical investigations were carried out.

For the present case, the total-flow formulation requires very long calculation times due to a slow convergence from the initially (arbitrarily chosen) attached boundary layer towards an almost time-periodic state of the flow field with a stable laminar separation bubble. Furthermore, such a simulation demands for a very high resolution due to the turbulent rear part of the separation bubble and requires a proper boundary-layer interaction model to capture the upstream influence of the entire LSB in the mean. Such a computation requires a supercomputer and will be discussed now.

4.1 Numerical Method for Direct Numerical Simulations

Spatial direct numerical simulation of the three-dimensional unsteady incompressible Navier-Stokes equations served to compute the flow field described above. The method uses finite differences of fourth/sixth-order accuracy on a Cartesian grid for downstream (NMAX) and wall-normal (MMAX) discretization (Kloker, 1998). Grid stretching in wall-normal direction allows to cluster grid points near the wall. In spanwise direction, a spectral ansatz is applied ($\mathsf{KMAX}+1$ modes). An explicit fourth-order Runge-Kutta scheme is used for time integration (LPER time steps per period of the fundamental disturbance). Upstream of the outflow boundary a buffer zone in the intervall $[x_{st,oBZ}, x_{en,oBZ}]$ smoothly returns the flow to a steady laminar state. Further details of the code *n3d*, i.e. the numerical method and the implementation, can be found in Meyer *et al.* (2003). Only a few adaptations compared to there have been made, namely the alteration of boundary conditions to allow for a total-flow formulation together with a boundary-layer interaction model.

4.2 Performance and Required Computational Resources

For the present resolution (see Table 1), the memory consumption and the performance observed is given in Table 3. A converged solution was achieved after 150 calculation periods, when mode $(\mathsf{0.5},\mathsf{0})$ – which can be viewed as a rough measure of low-frequency content in the flow – could be reduced to 10^{-3} in the first part of the LSB. This results in a computational time of $4619\,h$ on the NEC SX-6 and of $2517\,h (3175\,h)$ on the NEC SX-8 (MPI). The actual degree of vectorization was $\approx 95\%$ for 15 periods.

5 Conclusions

The present DNS method has proven capable of providing quantitatively space- and time-accurate simulations of (early) non-linear stages of a transition process in a LSB. This has been shown by means of a comparison with experimentally determined data. The non-linear transitional stages featured the formation of coherent structures, namely shear-layer roll-up and vortex shedding as shown by a visualization based on the spanwise vorticity. Correctly capturing these stages of transition is believed to be an essential condition for a simulation of (very) late stages with their complex interactions of disturbances. However, concerning the very late stages, additional calculations are necessary in the future to improve CFD results.

The high computational cost associated with the usage of supercomputers required for a DNS does not justify to apply these computers to merely demonstrate the capabilities and accuracy of a numerical method. Instead, by a mutual comparison of results from numerical (DNS), experimental, and theoretical methods, more profound insights into the flow physics can be gained for a certain flow situation then it would be possible if only one of these methods were applied. This aspect is one of the main benefits of such an approach, reaching beyond a mere verification of either the numerical, experimental, or theoretical method: it exploits the fact that all these methods do not only have different weaknesses, but of course also have different advantages.

The performance of the code for the present case was found satisfactory, with a maximum performance of 5.38 GLFOPS/CPU on the NEC SX-8 for a typical run. For the computations in disturbance formulation a suitable production server is somewhat lacking. These runs cannot make use of a large number of processors, so that PC-Clusters are not favorably applicable. Rather, serial runs (or runs with less than 6 CPUs) on a fast machine would be preferable, yet in that case often the sum of queue and production time almost exceeds the wall-clock time for the large-scale computation.

Acknowledgments

Financial support of this research by the Deutsche Forschungsgemeinschaft DFG under grant Wa 424/19–1 and Ri 680/10–1 is gratefully acknowledged. We thank Matthias Lang for providing detailed experimental results and Fredrik Svensson, NEC HPC Europe GmbH, for (past and ongoing) performance tuning on the DNS code *n3d* applied within the project LAMTUR.

References

Alam, M. & Sandham, N. D. 2000 Direct Numerical Simulation of 'Short' Laminar Separation Bubbles with Turbulent Reattachment. *J. Fluid Mech.* **410**, 1–28.

Kloker, M. 1998 A Robust High-Resolution Split-Type Compact FD Scheme for Spatial Direct Numerical Simulation of Boundary-Layer Transition. *Appl. Sci. Res.* **59**, 353–377.

Lang, M. 2005 Experimentelle Untersuchungen zur Transition in einer laminaren Ablöseblase mit Hilfe der Laser-Doppler-Anemometrie und der Particle Image Velocimetry. Dissertation, Universität Stuttgart.

Lang, M., Marxen, O., Rist, U. & Wagner, S. 2001 Experimental and Numerical Investigations on Transition in a Laminar Separation Bubble. In *New Results in Numerical and Experimental Fluid Mechanics III* (ed. S. Wagner, U. Rist, H.-J. Heinemann & R. Hilbig), *Notes on numerical fluid mechanics*, vol. 77, pp. 207–214. Contributions to the 12th STAB/DGLR Symposium, Nov. 15-17, 2000, Stuttgart, Germany, Springer, Heidelberg.

Lang, M., Rist, U. & Wagner, S. 2004 Investigations on controlled transition development in a laminar separation bubble by means of LDA and PIV. *Experiments in Fluids* **36**, 43–52.

Marxen, O. 2005 Numerical Studies of Physical Effects Related to the Controlled Transition Process in Laminar Separation Bubbles. Dissertation, Universität Stuttgart.

Marxen, O., Lang, M., Rist, U. & Wagner, S. 2003 A Combined Experimental/Numerical Study of Unsteady Phenomena in a Laminar Separation Bubble. *Flow, Turbulence and Combustion* **71**, 133–146.

Marxen, O., Rist, U. & Henningson, D. S. 2005 Steady three-dimensional Streaks and their Optimal Growth in a Laminar Separation Bubble. In *Contributions to the 14th STAB/DGLR Symposium, Nov. 16-18, 2004, Bremen, Germany*. Accepted for publication, Springer.

Marxen, O., Rist, U. & Wagner, S. 2004 Effect of Spanwise-Modulated Disturbances on Transition in a Separated Boundary Layer. *AIAA J.* **42** (5), 937–944.

Maucher, U., Rist, U. & Wagner, S. 2000 Refined Interaction Method for Direct Numerical Simulation of Transition in Separation Bubbles. *AIAA J.* **38** (8), 1385–1393.

Meyer, D., Rist, U. & Kloker, M. 2003 Investigation of the flow randomization process in a transitional boundary layer. In *High Performance Computing in Science and Engineering '03* (ed. E. Krause & W. Jäger), pp. 239–253. Transactions of the HLRS 2003, Springer.

Schlichting, H. 1979 *Boundary-Layer Theory*. McGraw-Hill, New York.

Spalart, P. R. & Strelets, M. K. 2000 Mechanisms of transition and heat transfer in a separation bubble. *J. Fluid Mech.* **403**, 329–349.

Watmuff, J. H. 1999 Evolution of a wave packet into vortex loops in a laminar separation bubble. *J. Fluid Mech.* **397**, 119–169.

Wissink, J. & Rodi, W. 2004 DNS of a laminar separation bubble affected by free-stream disturbances. In *Direct and Large-Eddy Simulation V* (ed. R. Friedrich, B. Geurts & O. Métais), *ERCOFTAC Series*, vol. 9, pp. 213–220. Proc. 5th internat. ERCOFTAC Workshop, Munich, Germany, Aug. 27-29, 2003, Kluwer Academic Publishers, Dordrecht, Boston, London.